Check for updates

Development of nanofibrous scaffolds by varying the TiO$_2$ content in crosslinked PVA for bone tissue engineering

Nandini A. Pattanashetti, Chinmay Hiremath, Satishkumar R. Naik, Geetha B. Heggannavar and Mahadevappa Y. Kariduraganavar [ID] *

The use of ceramic and metal nanoparticles is widely being proven as a preferred candidate for tissue engineering owing to their excellent properties such as their high penetration ability and high surface area with tuneable surface properties. In view of this, the effect of bioinert TiO$_2$ incorporation into the polymer matrix is studied in the present study. Crosslinked poly(vinyl alcohol) (PVA) was used as the main polymer base and different weight percentages of TiO$_2$ (0.1 to 0.3 g) were incorporated into the crosslinked PVA matrix by varying the ratio of PVA : TiO$_2$. Nanofibrous scaffolds were then fabricated using the electrospinning technique. The physicochemical properties of the developed nanofibrous scaffolds were analysed systematically. Scanning electron microscopy images demonstrated the good interconnected porous structure with uniform fibres in the range of several hundreds of nanometres. The effect of TiO$_2$ incorporation was observed in terms of an increase in the hydrophilicity of the scaffolds required for cellular infiltration. The mechanical characterization of the developed scaffolds demonstrated an improved mechanical strength for a reduced amount of TiO$_2$ incorporated scaffolds. The degradation study revealed the slow rate of degradation with an increase in the TiO$_2$ content in the PVA matrix of the scaffolds. Cell viability was studied using MG-63 bone osteosarcoma cells for 24, 48, 72 and 96 h, wherein the PT1 scaffold with a content of 0.1 g of TiO$_2$ exhibited the highest cell proliferation of 99.2%. The results thus clearly show that the TiO$_2$ incorporated PVA scaffolds could be potential candidates for bone tissue engineering.

1. Introduction

The multidisciplinary field of tissue engineering and regenerative medicine is in increasingly high demand in the present decade owing to the many drawbacks of tissue and organ transplantation, such as limited donor availability, the need for immune-suppression and insufficient success rate (rejection of the transplant). Tissue engineering is the development of artificial constructs known as scaffolds that can mimic the natural extracellular matrix (ECM), resembling natural tissues or organs provided with appropriate mechanical strength.[1] Scaffolds specifically developed for bone tissue engineering must possess a good-interconnected porous network with a large pore volume in order to ensure viable cell infiltration and attachment, and transportation of nutrients and waste products.[2,3] The geometry of scaffolds thus plays an important role in improving the overall properties. In order to incorporate the required

Department of Chemistry, Karnatak University, Dharwad, 580003, India.
E-mail: mahadevapaayk@gmail.com, kariduraganavrmy@kud.ac.in;
Fax: +91-836-2771275; Tel: +91-836-2215286

physical properties into the scaffolds many advanced scaffold fabrication techniques have been employed.[1] Recently, electro-spinning has been found to be an amazing method for the development of scaffolds in the form of nanocomposite fibres possessing nano structures.[4–7]

The material intended for scaffold development should be highly biocompatible with favourable surface properties for bone cell attachment and a large surface area-to-volume ratio for cell infiltration.[8,9] There are many biocompatible and biodegradable polymers used for bone tissue engineering applications, including (poly(L-lactic acid), poly(L-lactic-*co*-glycolic acid), poly(ε-caprolactone), poly(vinyl alcohol) (PVA) and poly(D,L-lactic acid)).[10] Among these, PVA is a biodegradable, biocompatible, nontoxic, and non-carcinogenic polymer which makes it an excellent biomaterial for bone tissue engineering. However, in addition to these properties, the highly hydrophilic PVA lacks the intrinsic mechanical properties that favour cell attachment, cell growth and differentiation. In order to overcome this, PVA was crosslinked with the minimum ratio of a non-toxic tetraethylorthosilicate (TEOS) crosslinker in the present study. The crosslinking of the PVA solution

thus enhances the stability of the electrospun nanofibres in aqueous media.

In order to accelerate bone tissue regeneration, inorganic–organic and polymer–inorganic composite based scaffolds are fabricated by many researchers that can mimic the composition and function of natural bone.[11,12] For instance, nanoparticles made up of various types of materials such as ceramics, metals, natural and synthetic polymers are one of the most widely preferred dopants in tissue engineering and regenerative medicine.[1,13,14] Nanoparticles play a contributory role in improving the mechanical strength of the scaffolds, providing a high penetration ability, a high surface area with tuneable surface properties and can act as bioink supplements and bioactive agents. In view of this, different weight percentages of titania nanoparticles were incorporated into the crosslinked PVA matrix in the present study in order to improve the mechanical properties of the developed scaffolds for bone tissue engineering. Titania (TiO_2) nanoparticles are bioinert nano-ceramics that are promising scaffolding materials for bone tissue repair.[15,16] TiO_2 scaffolds are considered to be cell carrier materials with a good permeability and high biocompatibility to enhance cell viability.[17–19] For instance, Tiainen et al., has investigated the in vivo performance in minipig jaws and observed an improved osteoconductive capacity for TiO_2 scaffolds.[20] Many researchers have proved that TiO_2 incorporation could improve the bioactivity and mechanical properties when coated with other polymers.[21–23] Similarly, Ikono et al. has developed chitosan scaffolds hybridized with TiO_2 nanoparticles in the form of sponges. As a result, a significantly improved sponge robustness, biomineralization, and bone regeneration capability was achieved.[23]

Thus, in the present study, different weight percentages of TiO_2 nanoparticles were introduced into the crosslinked PVA matrix and the nanofibrous scaffolds were developed using the electrospinning technique. The physicochemical properties of the developed nanofibrous scaffolds were studied systematically. The morphological characterization of the scaffolds was carried out using scanning electron microscopy (SEM). The water contact angle (WCA) measurements revealed the improved wettability of the TiO_2 incorporated composite scaffolds. The crystallinity of the scaffolds was analysed using X-ray diffraction (XRD) studies. The mechanical properties of the scaffolds were analysed using a universal testing machine. The cell viability and cell proliferation were studied on the scaffolds by performing the 3-(4,5-dimethylthiazolyl-2)-2,5-diphenyltetrazolium bromide (MTT) assay using MG-63 bone osteosarcoma cell lines.

2. Materials and methods

Poly(vinyl alcohol) (PVA) ($M_w \sim 125\,000$) and hydrochloric acid (HCl) were purchased from S. D. Fine Chemicals Ltd, Mumbai, India. TEOS was procured from E. Merck India Ltd, Mumbai, India. TiO_2 nanopowder was procured from Sigma Aldrich Chemicals, Germany. All of the chemicals were of reagent grade and used without further purification. Deionised distilled water was used throughout the experimental procedures. Dulbecco's phosphate buffered saline (DPBS), 0.25% trypsin–EDTA solution, MTT reagent and dimethyl sulfoxide (DMSO) were purchased from HiMedia, India. MG63 bone osteosarcoma cell lines were procured from the American type culture collection (ATCC), USA.

2.1 Preparation of the crosslinked PVA and TiO_2 composite material

Poly(vinyl alcohol) (4%) was dissolved in 50 ml of deionised distilled water under constant stirring at 60 °C for 2 h. The resulting solution was filtered and 0.4 ml of TEOS was added dropwise to the filtrate followed by the addition of HCl (0.5 ml) acting as a catalyst. The crosslinking ratio between PVA : TEOS was maintained at 1 : 0.2. The solution was stirred overnight at the same temperature. The schematic representation of PVA crosslinking with TEOS is shown in Scheme 1.

To the crosslinked solution, different weight percentages of TiO_2 were added by varying the ratio of PVA : TiO_2 from 1 : 0 to 1 : 0.15. Briefly, a known amount of TiO_2 nanopowder was added to a minimum amount of water under continuous stirring to obtain a dispersed TiO_2 solution. The resulting dispersed solution was slowly added to the crosslinked PVA solution while stirring. This was further stirred for 4 h to obtain a homogeneous solution. The resulting solution was then subjected to sonication so as to further enhance the dispersion of TiO_2 in the PVA solution. The resulting material compositions were designated as PT0, PT1, PT2 and PT3 throughout the study, as shown in Table 1. The schematic representation of TiO_2 incorporation into the crosslinked PVA matrix is shown in Scheme 2.

2.2 Electrospinning

The electrospinning technique was employed for the fabrication of nanofibrous scaffolds for all of the composite materials. The electrospinning setup is schematically represented in Fig. 1. Briefly, the solution was placed in a horizontally fixed 3 ml syringe pump with a metallic needle with an inner diameter
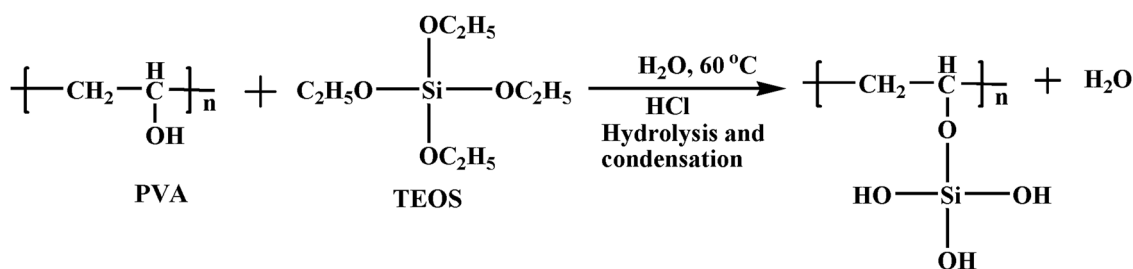
Scheme 1 Schematic representation of the acid catalysed crosslinking of PVA with TEOS.

Table 1 Different weight ratios of the PVA : TiO$_2$ composite materials

Sample	PVA (g)	TiO$_2$ (g)	PVA : TiO$_2$
PT0	2	0	1 : 0
PT1	2	0.1	1 : 0.05
PT2	2	0.2	1 : 0.1
PT3	2	0.3	1 : 0.15

of 0.55 mm. The flow rate of the spinning solution was maintained at 1 μl s^{-1} for all of the composite solutions. A rotating drum was employed as a collector at 800 rpm to collect the nanofibres. The applied voltage and tip-to-collector distance were 19 kV and 14 cm respectively. Electrospinning was performed at room temperature and 75% humidity. The electrospun PVA/TiO$_2$ nanofibres were collected on the aluminium foil wrapped on the rotating collector. The mat was removed and stored in a vacuum chamber for complete evaporation of the solvent for 48 h and then stored in a desiccator until further use.

3. Characterization

3.1 Fourier transform infrared spectroscopy

In order to confirm the crosslinking of PVA–TEOS and the nature of bonding among the composite blends of the crosslinked PVA and TiO$_2$ nanoparticles, Fourier transform infrared spectroscopy (FTIR) (Nicolet, Impact-410, USA) analysis was carried out for all of the composite nanofibrous scaffolds. The disc pellets were prepared by grinding the nanofibres thoroughly with potassium bromide. The IR spectra of the pellets were then analysed using an FTIR spectrometer operating at a range of 400–4000 cm^{-1}.

3.2 Thermogravimetric analysis

The thermal stability of the composite materials was investigated using PerkinElmer TGA/DTA thermogravimetric analyser (SDT Q600, TA Instruments-Waters LLC, USA). During thermogravimetric analysis (TGA), about 8–10 mg of the sample was heated from ambient temperature to 600 °C at a rate of 10 °C min^{-1} under a constant flow of nitrogen gas (100 ml min^{-1}).
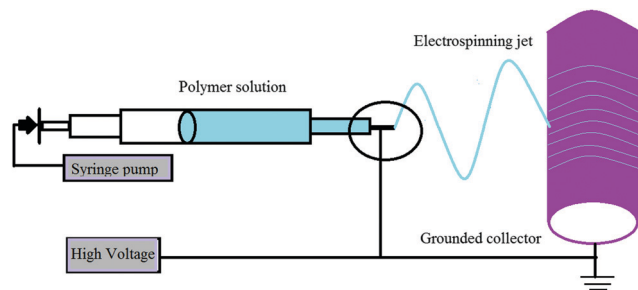
Fig. 1 Illustration of the electrospinning set-up.

3.3 X-ray diffraction spectroscopy

The XRD analysis was performed using a powder X-ray diffractometer (RIGAKU Smartlab, Japan) at room temperature. The X-ray source was Ni-filtered Cu-Kα radiation (40 kV, 30 mA). The samples were mounted on a sample holder and diffraction was scanned in the reflection mode at an angle of 2θ over a range of 10–80° at a constant speed of 5° min^{-1}.

3.4 Scanning electron microscopy

The morphology of the developed electrospun scaffolds was investigated using SEM (JSM-IT500 JEOL, USA). The samples were sputter coated with a thin layer of gold using a Neocoater for about 60 seconds at 10^{-6} mbar pressure and a process current of 10 mA. The average diameter of the electrospun nanofibres was measured using *Image J* software.

3.5 Wettability measurements of the scaffolds

The hydrophilicity of the nanofibrous scaffolds was measured using a sessile drop method at room temperature using a Static Contact Angle Goniometer (Kyowa Interface Science Co. Ltd, Agram Industries, Japan) using FAMAS software. Drops of distilled water (3 μl) were deposited on the nanofibrous mat and the incident contact angle was directly measured using the software. The measurements were made at five different positions of the sample and the mean ± SD was thereby calculated.

3.6 Mechanical testing of the scaffolds

The mechanical strength of the electrospun nanofibrous mat was determined using a universal tensile testing machine (UTM)
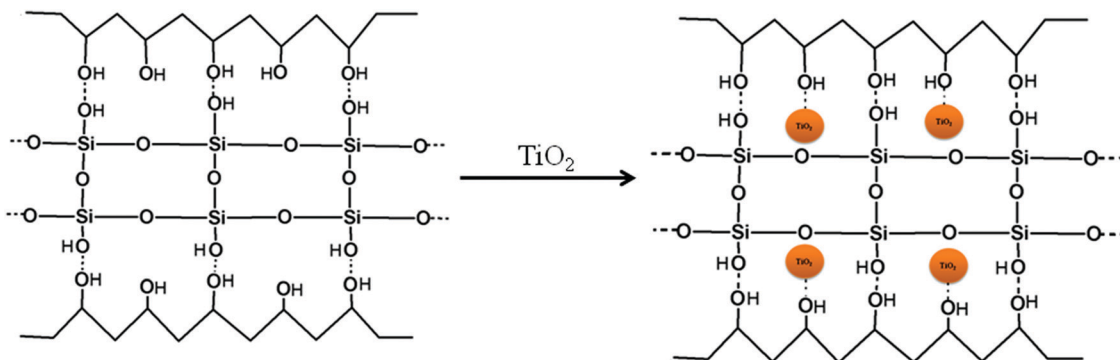
Scheme 2 Schematic representation of TiO$_2$ incorporation into the crosslinked PVA matrix.

(Dak System Inc., Mumbai, India) at room temperature. The composite samples were cut into a rectangle with the dimensions of 2×10 cm and the thickness of each sample was measured under dry conditions using a Peacock dial thickness gauge (Model G, Ozaki MFG. Co. Ltd, Japan). The resulting thickness of the samples was found to be in the range of 20–30 μm. The scaffold samples were then placed at the jaws of the UTM and stretched from both the ends at a rate of 0.1 mm min^{-1} by applying a load of 1 kN until break. Four specimens of each scaffold sample were tested to determine the mechanical strength and the mean stress–strain curves were plotted. The average Young's modulus value was calculated from the linear elastic region of the stress–strain curves.

3.7 Bio-degradation study of the scaffolds

The rate of degradation of the PT0, PT1, PT2 and PT3 composite scaffolds was studied in phosphate buffer saline (PBS) solution with a pH of 7.2. Scaffolds of equal weight were immersed in PBS solution (2 ml) and incubated at 37 °C for 7 d. The observations were made for seven different time intervals for up to 7 d. The initial weight of the scaffold was noted as W_0. After regular time intervals, the sample was removed from PBS and washed in deionised water to remove the adsorbed ions on the surface. Furthermore, the sample was dried using filter paper and the dried weight was noted as W_t. The degradation of the scaffold was calculated using the formula given in eqn (1).[24]

$$\text{Degradation\%} = \frac{W_0 - W_t}{W_0} \times 100 \qquad (1)$$

3.8 Cytotoxicity study of the scaffolds

The cytotoxicity of the scaffolds was studied by extract assay using the MTT test system. The nanofibrous scaffolds were washed with ethanol (70%) several times and sterilized under ultraviolet (UV) light for 15 min. 50 mg of scaffold materials were extracted in 30 ml culture medium containing Dulbecco's modified Eagle's medium with high glucose (DMEM-HG) supplemented with 10% fetal bovine serum (FBS) at 37 °C for 24 h. These were considered to be the test solutions and assayed further. MG-63 cells were cultured, trypsinized and centrifuged to obtain a cell pellet. The cell count was adjusted using DMEM-HG supplemented with 10% FBS to obtain 10 000 cells/200 μl of cell suspension. This cell suspension was then added into each well of the 96 well microtitre plate and incubated at 37 °C under a 5% CO$_2$ atmosphere for 24 h. After 24 h, the spent medium was aspirated and 200 μl of the test solutions were added to the respective wells. The plates were then incubated at 37 °C under a 5% CO$_2$ atmosphere for 24, 48, 72 and 96 h. After each time interval the MTT test was performed. The yellow tetrazolium MTT was reduced by the metabolically active cells and the resulting intracellular purple formazan was solubilized in DMSO and quantified by spectrophotometric means. The absorbance was measured using a microplate reader at a wavelength of 570 nm.

3.9 Statistical analysis

All of the data were presented as mean $\pm$ standard deviation (SD). One-way analysis of variance (ANOVA) (Fisher's LSD test)

was used to conduct the statistical analysis between each group unless otherwise indicated. $p < 0.05$ was considered significant. All of the quantifications were carried out on high resolution images using *Image J* software. A confidence level was set as 95% for $p^* < 0.05$.

4. Results and discussion

4.1 FTIR analysis

In the present study, PVA was employed as a base polymer for the development of scaffolds using the electrospinning technique. However, the electrospun PVA nanofibers possess a very high water-solubility which limits their applications. In contrast, chemical crosslinking can improve the stability of PVA in the aqueous media and can improve its mechanical properties.[25] The chemical crosslinking of PVA has been well studied using TEOS and has revealed that the hydroxyl groups of PVA and the precursors of TEOS react with each other in the presence of a strong acid.[26] Therefore, in the present study, a crosslinked PVA solution was prepared using TEOS as a crosslinking agent at an elevated temperature and the effect of TiO$_2$ incorporation in the polymer matrix was systematically studied. The crosslinking between PVA–TEOS and the immobilization of TiO$_2$ in the crosslinked PVA matrix was confirmed by FTIR study. The incorporation of the silicon groups of TEOS into the PVA matrix was confirmed by the IR spectra as shown in Fig. 2. A characteristic broad band appearing around 3400 cm^{-1} corresponds to the –OH stretching vibrations of the hydroxyl groups of PVA. The band observed around 2906 and 1730 cm^{-1} corresponds to the alkyl group (–CH$_2$) and the acetyl group of PVA respectively. Furthermore, multiple bands appearing at 1000–1100 cm^{-1} are assigned to the C–O stretching of PVA and also the Si–O stretching of TEOS. The bands of Si–O around 1100 cm^{-1} were found to be overlapping with the bands for C–O stretching. This suggests the formation of a Si–O–C bond which gives evidence for the crosslinking of PVA with TEOS. On the
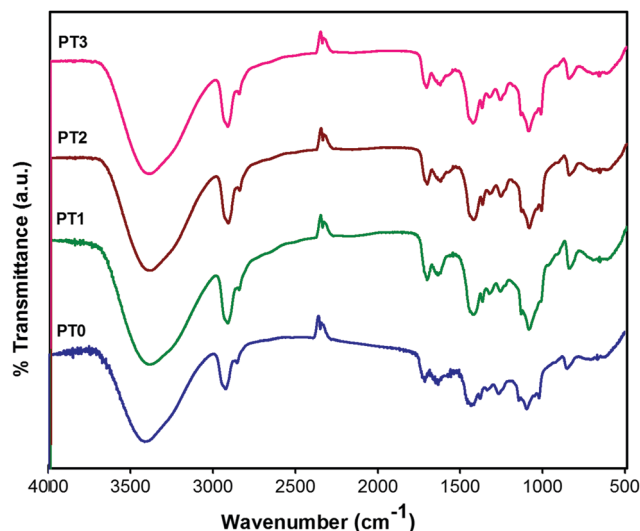

Fig. 2 The FTIR spectra of the composite nanofibrous scaffolds.

other hand, no new bands appeared in the infrared spectroscopy (IR) spectrum to show the bonding between TiO$_2$ and the crosslinked PVA matrix. However, the bands around 3400 cm^{-1} were slightly shifted towards a higher wavenumber which may be attributed to the interaction between the hydrophilic TiO$_2$ and PVA matrix. This indicates the incorporation of TiO$_2$ nanoparticles into the PVA matrix.

4.2 Thermogravimetric analysis

Thermogravimetric analysis was performed to determine the effect of TiO$_2$ incorporation on the thermal stability of the developed nanofibrous scaffolds and the resulting thermograms are shown in Fig. 3. The initial weight loss in all of the scaffolds was due to the volatilization of the physically absorbed water or moisture. For PT0, it can be seen that PVA was stable up to 255 °C and the decomposition occurred above 265 °C. The second step of decomposition occurred between 350–400 °C with an increased weight loss percentage. However, in the case of the TiO$_2$ incorporated scaffolds (PT1, PT2 and PT3), the decomposition occurred at marginally higher temperatures ranging from 270 to 290 °C owing to the efficient incorporation of TiO$_2$ into the composite matrix. The overall weight loss percentage for these scaffolds was observed to be lower when compared to the PT0 nanofibrous scaffold. This suggests a lower degradation potential and a higher temperature stability for the TiO$_2$ incorporated composite scaffolds even at a higher temperature range. This is attributed to the homogeneous loading of TiO$_2$ nanoparticles in the PVA matrix which thereby establishes a strong interaction between the PVA and nano-sized TiO$_2$ particles. This results in the increased thermal stability of the resulting composite scaffolds.

4.3 X-ray diffraction spectroscopy

To analyse the crystalline structure of the crosslinked PVA scaffold and the TiO$_2$ incorporated composite scaffolds, X-ray diffraction was studied and the resulting spectra are shown in Fig. 4. It was observed that the XRD patterns revealed a sharp intense diffraction peak at $2\theta = 19.5°$ for the PT0 scaffold, which reveals the clear
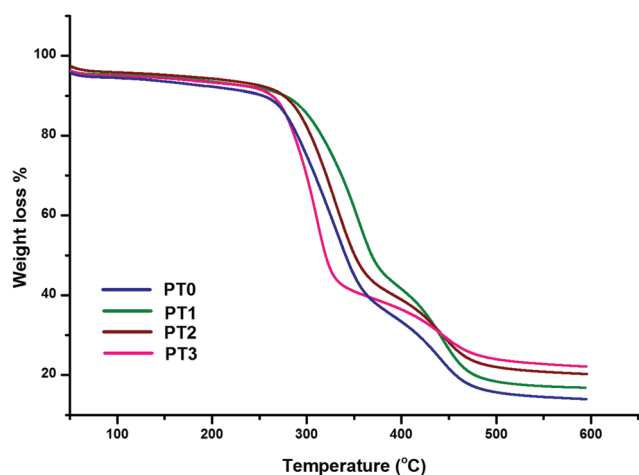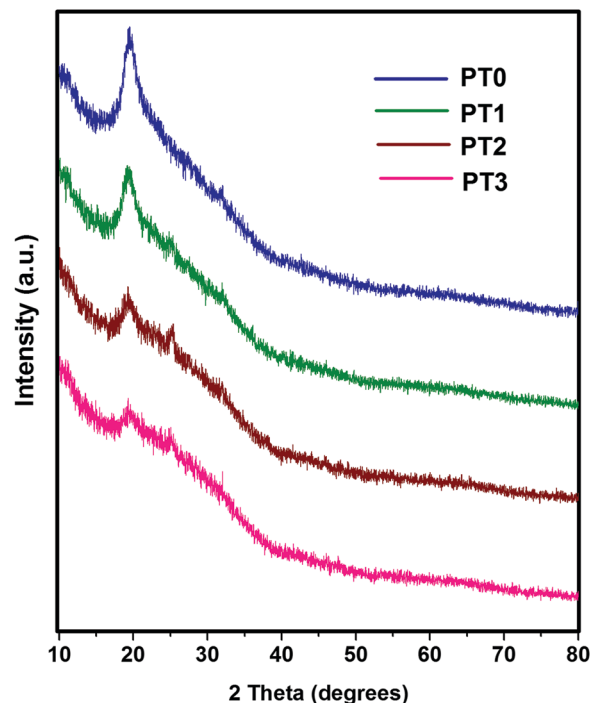

Fig. 4 The XRD spectra of the composite nanofibrous scaffolds.

crystalline nature of the crosslinked PVA nanofibres. The intensity of this diffraction peak was observed to decrease for the TiO$_2$ incorporated PT1, PT2, and PT3 scaffolds. This change in the peak intensity clearly indicates the presence of TiO$_2$ nanoparticles in the crosslinked PVA composite matrix. The reduced peak intensity and broadening of the area under the peak for TiO$_2$ incorporated scaffolds reveals the decrease in the crystallinity of the scaffolds. This is attributed to the presence of a greater amount of hydrogen bonding between the hydrophilic TiO$_2$ and PVA matrix with an increase in the TiO$_2$ content. This is well supported by the results of the FTIR study in which the –OH shifts towards a higher wavenumber. However, these scaffolds also exhibited an additional weak peak at $2\theta = 25.4°$ corresponding to the TiO$_2$ crystal structure. This shows that the TiO$_2$ nanoparticles are homogenously incorporated into the PVA matrix. Thus, it was concluded that the increase in TiO$_2$ content has eventually increased the flexibility of the crosslinked PVA polymer chains thereby increasing the degree of amorphousity.

4.2 Morphology observation of the scaffolds

An important aspect of tissue engineering lies in the design of polymeric scaffolds similar to the native ECM in order to modulate cellular behaviour. The scaffold should be porous with a high surface area-volume ratio to allow cell attachment and cell in-growth, as well as the exchange of nutrients during *in vitro* or *in vivo* culture. Thus, by using the electrospinning technique the required physical properties of the scaffolds could be achieved. In view of this, electrospun scaffolds were fabricated in the present study for bone tissue engineering.

The scanning electron microscopic images of the crosslinked PVA and TiO$_2$ incorporated composite nanofibrous scaffolds

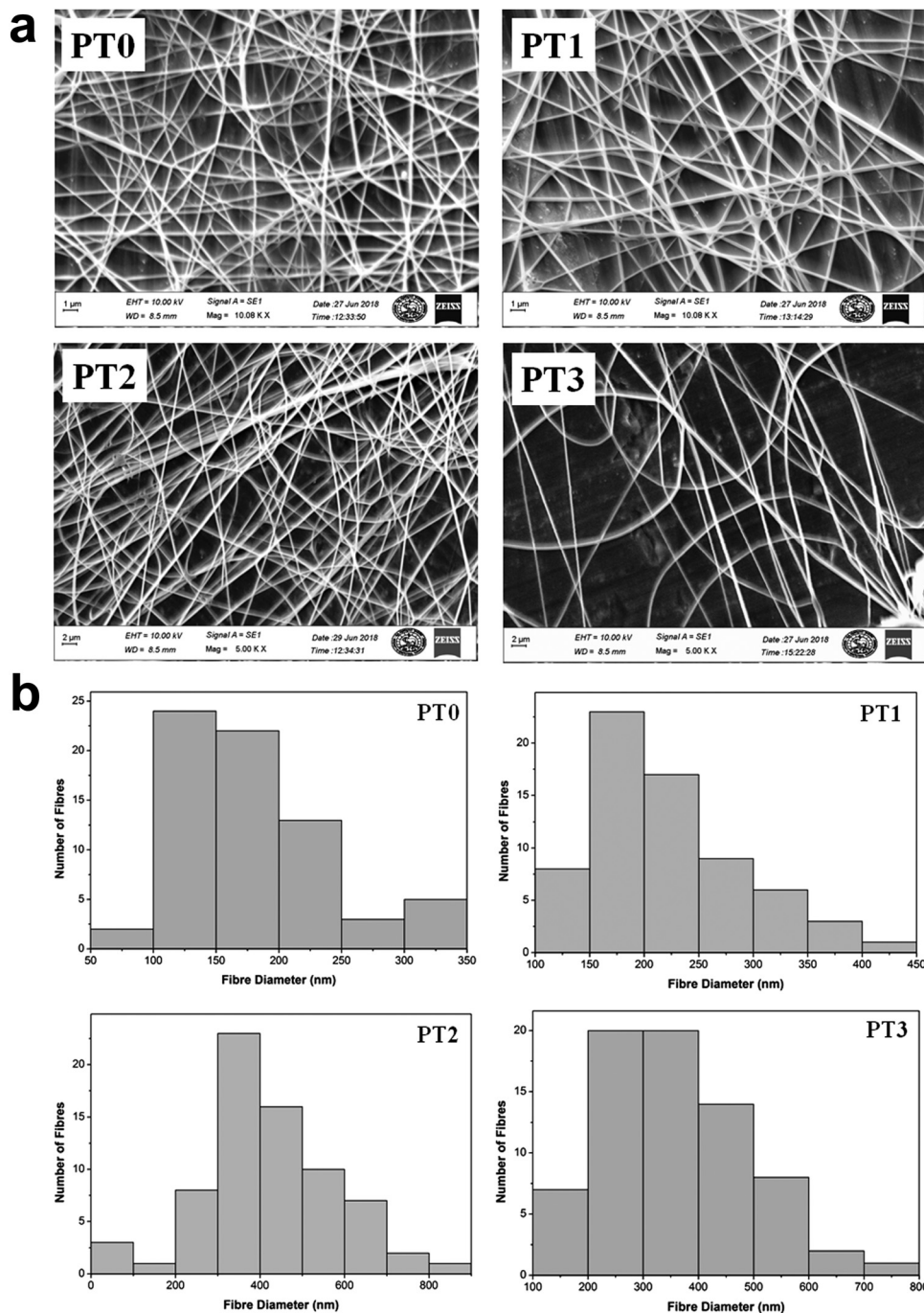Fig. 3 The TGA thermograms of the composite nanofibrous scaffolds.

Fig. 5 (a) SEM images of the nanofibrous scaffolds. (b) Histogram analysis of the electrospun nanofibres of the composite materials.

are shown in Fig. 5a. It can be seen that the morphology of the developed scaffolds exhibited fine, smooth and uniform fibres for all the composite scaffolds. There were no signs of agglomerations or bead formation owing to TiO_2 incorporation in the nanofibrous scaffolds. This shows that the TiO_2 nanoparticles were homogeneously and uniformly distributed into the cross-linked PVA matrix. Fig. 5b shows the histogram analysis of the electrospun scaffolds which reveals that the fibre diameter had a range of several hundred nanometers with a smooth surface. In particular, the fibre diameter was estimated to be 175.9 ± 59,

223.43 ± 66, 365.38 ± 132 and 379.52 ± 160 nm for the PT0, PT1, PT2 and PT3 scaffolds respectively. Thus, it was observed that the fibre diameter increased with an increase in the TiO_2 content in the polymer matrix, which can be attributed to the increase in the viscosity of the solution owing to an increase in the TiO_2 content in the PVA matrix. Fig. 6 shows the SEM images of the electrospun nanofibrous mats. From the images, it was observed that there were some agglomerations owing to the higher content of TiO_2 incorporation in the PVA matrix due of continuous overlapping of the electrospun nanofibres.
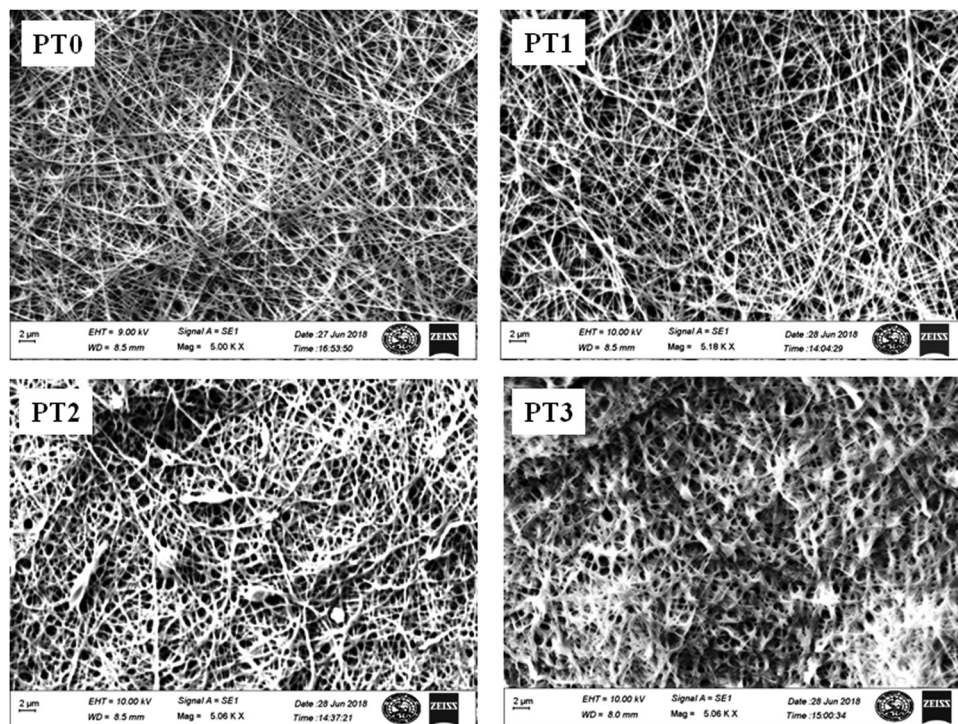
Fig. 6   SEM images of the nanofibrous mat.

In addition, with an increase in the TiO_2 incorporation, the surface roughness of the nanofibrous mat was also increased.

4.3   Wettability of the scaffolds

The wettability of the developed nanofibrous scaffolds was determined by measuring the WCA upon the samples. As it is a well-known fact that PVA is a hydrophilic polymer, all of the scaffolds exhibited lower WCA values of $<90°$ as shown in Fig. 7. In addition to this, the TiO_2 incorporated nanofibrous composite scaffolds possessed significantly lower WCA values when compared to the PT0 scaffold. The WCA measurement was decreased from $66°$ for PT0 to $59°$ for PT3 respectively. This was expected because TiO_2 is considered as a superhydrophilic material owing to the fact that a greater number of –OH groups will be available in the matrix for the formation of hydrogen bonding with the water molecules in PT1, PT2 and PT3
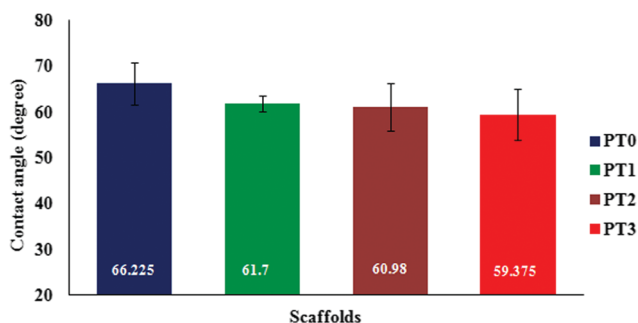
scaffolds successively. In addition, the increase in the surface roughness, as evidenced by the SEM images of the nanofibrous mats, also played an important role in the increasing wettability of the scaffolds. Based on this result, we conclude that the hydrophilicity of the scaffolds was greatly improved by the addition of TiO_2 content in the PVA matrix. In a similar study by Kiran et al.,[27] the effect of TiO_2 incorporation was studied by the incorporation of different weight percentages of TiO_2 in the polycaprolactone (PCL) matrix, in which the hydrophilicity of the PCL/TiO_2 scaffolds was decreased from $140°$ to $60°$ owing to the incorporation of superhydrophilic TiO_2.

4.4   Mechanical properties of the scaffolds

The polymeric nanofibrous scaffolds must possess adequate mechanical strength to support the cell growth and tissue organization over the scaffolds. It was observed that the mechanical properties of the scaffolds depend on the concentration of the incorporated TiO_2 particles. Fig. 8 shows the average stress–strain curves of the composite scaffolds. The tensile strength, elongation at break and elastic modulus were calculated based on the stress–strain curves of the composite scaffolds as shown in Table 2. It was observed that the incorporation of TiO_2 into the crosslinked PVA matrix had an effect on the elongation at break percentage values. With the increase in the TiO_2 content in the crosslinked PVA matrix, the strain at break values were increased. This reveals that the rigidity of the scaffolds was greatly influenced by the higher amount of TiO_2 incorporation in the matrix in terms of an increase in the elongation at break percentage values of the PT1, PT2 and PT3 composite scaffolds as compared to PT0. This is explained based on the reduced crystallinity of the scaffolds as observed from the XRD data.
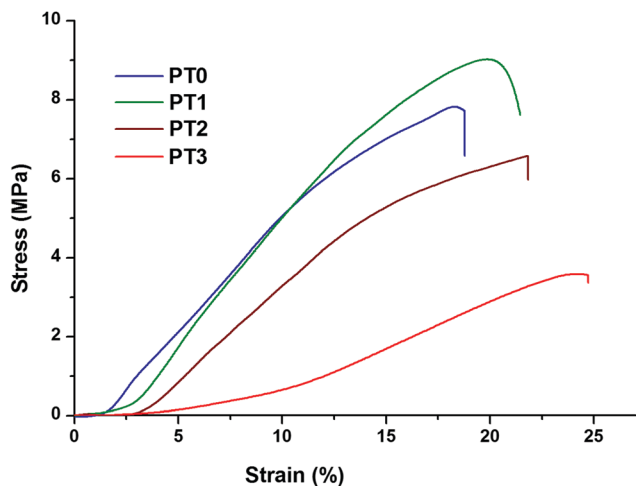

Fig. 7   The contact angle measurements of the $PVA:TiO_2$ composite scaffolds (data presented as mean $\pm$ SD).

Fig. 8 The stress–strain curves of the PVA/TiO$_2$ composite scaffolds.

Table 2 The mechanical properties of the PVA : TiO$_2$ composite scaffolds

Scaffold name	Elongation at break (%)	Tensile strength (MPa)	Young's modulus (MPa)
PT0	17.38	7.57	58.82
PT1	19.88	9.01	68.05
PT2	21.85	6.51	58.45
PT3	24.89	3.76	34.31

Furthermore, an improved mechanical property of the TiO$_2$ incorporated scaffold was observed for the PT1 scaffold in terms of the Young's modulus (68.05 MPa) and the tensile strength (9.01 MPa) values. These values were remarkably higher than the PT0 scaffold without TiO$_2$ content. However, with the further increase in the TiO$_2$ content for the PT2 and PT3 scaffolds, the mechanical properties decreased as shown in Table 2. This decrease in mechanical strength and the increase in the elongation at break values of the scaffolds are attributed to the increase in amorphousity of the TiO$_2$ incorporated composite scaffolds. The weak hydrogen bonds of the amorphous scaffolds reduced the mechanical properties of the PT2 and PT3 scaffolds in particular. Thus, it can be concluded that the addition of a lower amount of TiO$_2$ (0.1 g) is desirable and sufficient to gain the mechanical strength of the developed composite scaffolds. Accordingly, an improved mechanical strength was observed only for the PT1 scaffold. However, the previously published literature states that the incorporation of TiO$_2$ nanofiller enhances the mechanical strength of the resulting composites, but in the present study this was only proved to be true for the PT1 scaffold.

4.5 Bio-degradation study of the scaffolds

The rate of degradation of the scaffolds is another very crucial parameter that needs to be considered, specifically for bone tissue engineering. The controlled rate of degradation of the scaffolds provides space for the tissue in-growth and matrix deposition. The *in vitro* degradation study was carried out using a traditional assay with a PBS solution of pH = 7.2. The scaffolds were incubated in PBS solution for 1 week and the rate of degradation was calculated in terms of the weight loss percentage after every
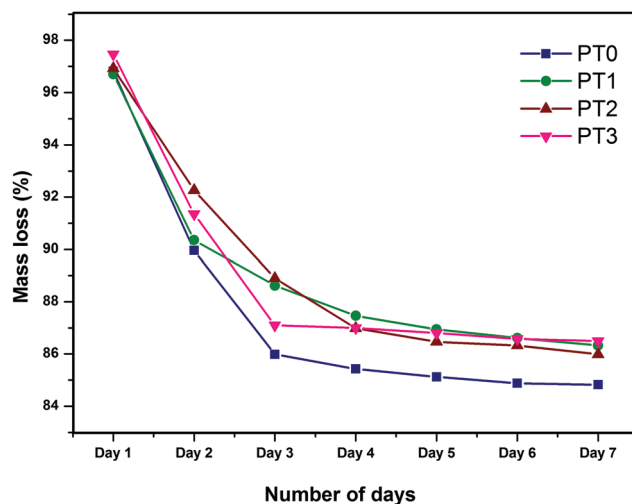

Fig. 9 Degradation study for the PVA : TiO$_2$ composite nanofibrous scaffolds.

24 h up to 7 d, the data is shown in Fig. 9. It was observed that the rate of degradation decreased from day 1 to day 7 for all of the scaffolds. Specifically, all of the scaffolds exhibited a considerable mass loss during day 1 to day 3, whereas no considerable difference in the weight loss was found during the next 3 d among the samples. This could be due to the leaching out of loosely bonded TiO$_2$ molecules during the first three days of degradation. The graphs reached a plateau during the next 4 to 7 days of the degradation period. Furthermore, on comparing PT0 with the TiO$_2$ incorporated composite scaffolds, it was observed that the rate of degradation was marginally slow for the PT1, PT2 and PT3 scaffolds during day 4 until day 7. The slower degradation rate of the PVA : TiO$_2$ composite scaffolds can be attributed to the increase in the stability of the scaffolds owing to the increase in the TiO$_2$ content. Thus, the results show that the TiO$_2$ incorporated PVA composite scaffolds possess suitable degradation properties for bone tissue engineering.

4.6 Cytotoxicity study of the scaffolds

The cell viability of the composite scaffolds was carried out using MG-63 bone osteosarcoma cell lines during 24, 48, 72 and 96 h culture times. The cells were cultured onto the scaffold extracts and an MTT assay was performed to investigate the biocompatibility of the scaffolds in terms of the cell proliferation percentage. Fig. 10a–d shows the optical microscopic images of the cells grown on all of the nanofibrous scaffolds after 24, 48, 72 and 96 h of cell proliferation respectively. From the microscopic images a uniform growth of cells could be observed in all of the composite nanofibrous scaffolds with no evidence of any toxic effects and cell death.

Fig. 11 shows the similar observations in terms of the calculated absorbance values of cell proliferation studies recorded after every 24 h up to 96 h. From the data, it is clear that all of the scaffolds exhibited an increase in the cell proliferation percentage with due time from 24 to 96 h. On comparing PT0 with the TiO$_2$ incorporated scaffolds, PT0 demonstrated 97.27% of cell proliferation after 96 h. PT1 demonstrated a marginally greater
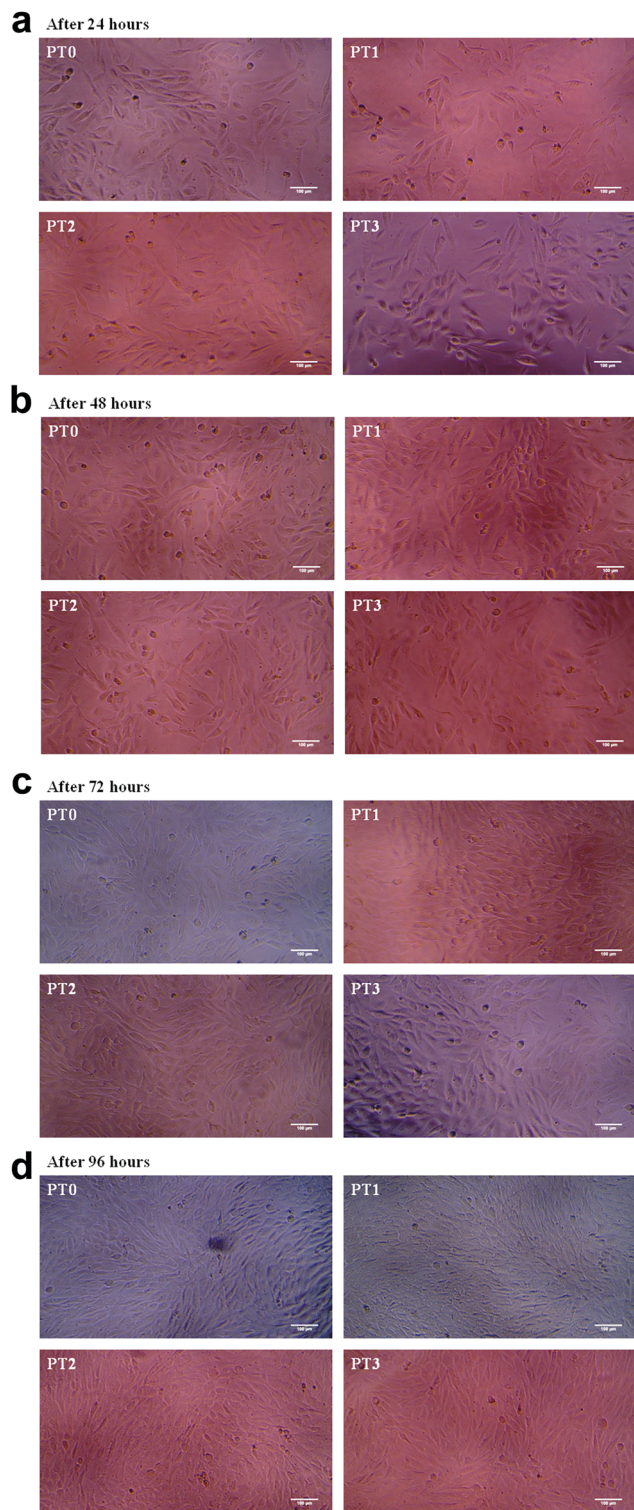
a After 24 hours

b After 48 hours

c After 72 hours

d After 96 hours

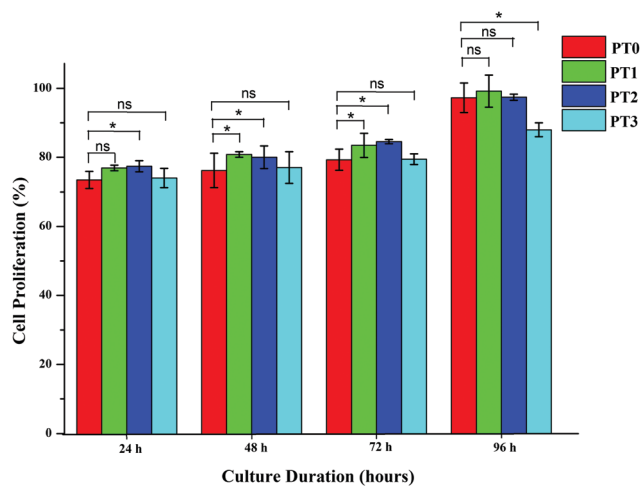Fig. 10   (a) Microscopic images of cell proliferation after 24 h, (b) 48 h, (c) 72 h and (d) 96 h.

Fig. 11   Cell proliferation of the composite nanofibrous scaffolds ($p* < 0.05$).

cell proliferation of the MG-63 bone osteosarcoma cells compared to PT2 and PT3. However, some inhibitory effect was observed in the case of the PT3 scaffold with a greater amount of TiO_2 content. This may be attributed to the increase in the surface roughness of the scaffolds as observed by the SEM analysis. The increase in the surface roughness of the scaffolds might have reduced the uniformity of the pores on the surface and in the bulk, which thus hinders the proper growth and infiltration of cells into the scaffold. However, this decrease can be considered insignificant because there were no cell deaths observed. Therefore, we can conclude that the developed scaffolds with the incorporation of the TiO_2 nanofiller in the crosslinked PVA matrix are cell-viable and biocompatible in nature with no signs of toxic effects for bone tissue regeneration.

4.7   Comparison study of PVA based electrospun nanofibrous scaffolds

Poly(vinyl alcohol) is a water soluble and bio-absorbable polymer, and it is thus compatible with human tissues. The development of PVA based nanofibrous scaffolds by the electrospinning process has been investigated by many researchers owing to its visco-elastic properties. However, the electrospun PVA scaffolds are equally associated with some limitations such as a high water solubility and poor mechanical strength, which restrict their application for bone tissue engineering. In order to overcome this, the crosslinking method was employed to improve the stability of the scaffolds. Many researchers have employed different crosslinking methods such as vapour crosslinking, thermal crosslinking, *in situ* crosslinking and post crosslinking to stabilise the scaffolds. In all of these methods, glutaralde-hyde was used as a crosslinker, which itself has toxic effects on the cells.[28–30] To overcome this problem, we employed TEOS as a crosslinker and crosslinked the PVA solution prior to the scaffold fabrication. With the precursor of silica, TEOS is a non-toxic and biocompatible crosslinker which does not produce any cytotoxic effects during cell culture. Furthermore, different weight percentages of TiO_2 were incorporated into the PVA matrix in order to improve the properties of the scaffolds for

cell proliferation percentage of 99.2%, whereas PT2 and PT3 respectively showed 97.43% and 87.97% of cell proliferation after 96 h. Although all of the scaffolds demonstrated an increase in cell proliferation during 96 h of cell cultures, in particular, PT1 with a lower amount of TiO_2 content revealed a superior

bone tissue engineering. As a result, the developed scaffolds exhibited smooth and uniform fibres.

The morphology and mechanical properties of the scaffolds plays a significant role in their applications in bone tissue engineering. The fibre diameter determines the overall porosity of the scaffolds for cell growth and proliferation. In a study by Jamnongkan *et al.*,[31] the average fibre diameter of PVA was found to be 1059 nm, which is much higher than the average fibre diameter (176 nm) of the crosslinked PVA fibres developed in the present work. Furthermore, the PVA/chitosan (95/5) and PVA/chitosan (90/10) composite scaffolds demonstrated average diameters of 823.6 and 799.4 nm, respectively. Upon comparing the average fibre diameters of the scaffolds with the present study, the TiO_2 incorporated scaffolds exhibited significantly lower fibre diameters. The incorporation of TiO_2 does not affect the morphology of the fibres and smooth and bead-free fibres were therefore obtained. In contrast to this, Nasikhudin *et al.*[29] also observed the distribution of TiO_2 nanoparticles on the surface of PVA fibres in the form of agglomeration and beads. In a study by Kyu-Oh Kim *et al.*,[30] the post crosslinking method was used on electrospun PVA nanofibres using glutaraldehyde (GA). It was observed that the average fibre diameter of the pure PVA and crosslinked PVA were 430 and 400 nm, respectively, wherein GA did not significantly influence the fibre diameter of the scaffolds. In contrast, the fibre diameter of the TEOS crosslinked PVA fibres was significantly affected.

In addition to this, the effect of TiO_2 incorporation was also studied in terms of the improved mechanical properties of the developed scaffolds. Although the tensile strengths of TiO_2 incorporated PVA scaffolds were comparable with the literature values, the tensile strength of the PT1 scaffold in particular exhibited a significantly higher value than those of the other PVA based nanofibrous scaffolds reported in the literature.[29,32–34] It was found that a suitable amount of TiO_2 incorporation into the PVA matrix was sufficient to enhance the tensile strength (up to 9.01 MPa) of the scaffolds. For instance, in a study by Saber-Samandari *et al.*,[19] TiO_2 was incorporated into cellulose–polyacrylamide/hydroxyapatite scaffolds. The resulting mechanical characterization revealed that a compressive strength of 1 g TiO_2 and 4 g TiO_2 incorporated into PVA scaffolds showed a result of 1.6 and 4.1 MPa, respectively. Similarly, in a study by Linh and Lee,[33] the properties of uncrosslinked and crosslinked PVA/gelatin scaffolds were evaluated and it was noted that the tensile strengths of the uncrosslinked and crosslinked PVA/gelatin scaffolds were 3.55 and 4.20 MPa, respectively. However, in the present study, the crosslinked PVA scaffold (PT0) and TiO_2 incorporated crosslinked (PT3) scaffolds were respectively found to be 7.57 and 3.76 MPa.

Based on the above discussion, we conclude that the developed nanofibrous scaffolds in the present study could provide suitable characteristic features in terms of the morphology and mechanical strength for bone tissue engineering. Furthermore, the extent of cell growth and cell proliferation depends on the variable features of the scaffolds, such as the fibre diameter, pore size, porosity, nature of the material and the cell culture duration.

Thus, researchers generally attempt to vary these characteristic features of the scaffolds in order to achieve maximum cell proliferation during the stipulated culture time. Keeping this in mind, we have made an attempt to achieve considerable cell growth without imposing any toxic effects during a 96 h cell culture study.

5. Conclusions

In the present study, nanofibrous composite scaffolds were developed using the electrospinning technique. PVA was crosslinked with TEOS in a smaller ratio (1 : 0.2) in order to improve its stability in aqueous media and also to enhance the mechanical properties. The stable crosslinked PVA was incorporated with different weight percentages of TiO_2 in order to study the influence of the TiO_2 content on the developed scaffolds. The incorporation of TiO_2 has greatly enhanced the thermal stability of the resulting scaffolds, as obtained using TGA thermograms. The developed scaffolds exhibited a highly porous structure with uniform fibres with diameters within several hundred nanometers, as evidenced by SEM images. These porous nanofibrous scaffolds resulted in an increase in the hydrophilic nature of the scaffolds in terms of the lower contact angle values with the increase in the TiO_2 content in the PVA matrix. This was explained by the formation of hydrogen bonding with the water molecules. The reduced amount of TiO_2 nanoparticle incorporation has formed a strong interface with the PVA matrix, which has demonstrated the improved mechanical strength of the PT1 scaffold when compared to PT0 and other composite scaffolds. This was explained by the existence of the crystalline nature of the PT1 composite scaffold compared to the other amorphous PT2 and PT3 scaffolds. This revealed that a small amount of TiO_2 incorporated into the PVA matrix is adequate to enhance the mechanical stability of the scaffolds. The slower degradation rate plays a prime role in bone tissue regeneration. In the present study, a marginally slow rate of degradation was observed for the TiO_2 incorporated scaffolds during the 7 days of the degradation study. Furthermore, the developed scaffolds were proved to be viable and non-toxic to the cells, as observed by the MTT assay using MG-63 bone osteosarcoma cell lines. The incorporation of TiO_2 content into the crosslinked PVA matrix and the resulting good porous structure of the nanofibrous scaffolds demonstrated a remarkable increase in the cell proliferation for all of the scaffolds as evidenced during the duration of the 96 h culture. A slower rate of cell proliferation was also observed for the scaffold with a higher content of incorporated TiO_2. On the whole, PT1 with a small amount (0.1 g) of TiO_2 incorporated into the crosslinked PVA matrix exhibited an improved thermal stability, mechanical strength and considerably enhanced cell proliferation percentage when compared to the PT0, PT2 and PT3 scaffolds. Thus, the PT1 scaffold was proven to be the most suitable candidate for bone tissue engineering. On this basis, a further detailed *in vivo* study is recommended in our future studies.

Conflicts of interest

There are no conflicts to declare.

Acknowledgements

References

1   K. Huang, J. Hou, Z. Gu and J. Wu, *ACS Biomater. Sci. Eng.*, 2019, **5**, 5384–5391.

2   D. W. Hutmacher, *Biomaterials*, 2000, **21**, 2529–2543.

3   J. R. Jones and L. L. Hench, *Curr. Opin. Solid State Mater. Sci.*, 2003, **7**, 301–307.

4   D. W. Hutmacher, J. T. Schantz, C. X. F. Lam, K. C. Tan and T. C. Lim, *J. Tissue Eng. Regener. Med.*, 2007, **1**, 245–260.

5   A. C. Jones, C. H. Arns, D. W. Hutmacher, B. K. Milthorpe, A. P. Sheppard and A. Knackstedt, *Biomaterials*, 2009, **30**, 1440–1451.

6   J. X. Lu, B. Flautre, K. Anselme, P. Hardouin, A. Gallur, M. Descamps and B. Thierry, *J. Mater. Sci.: Mater. Med.*, 1999, **10**, 111–120.

7   T. S. Karande, J. L. Ong and C. M. Agrawal, *Ann. Biomed. Eng.*, 2004, **32**, 1728–1743.

8   A. Greiner and J. H. Wendorff, *Angew. Chem., Int. Ed.*, 2007, **46**, 5670–5703.

9   B. Ding, M. Wang, X. Wang, J. Yu and G. Sun, *Mater. Today*, 2010, **13**, 16–27.

10 N. A. Pattanashetti, C. Hiremath, N. Alves and M. Y. Kariduraganavar, Advances in Polymers and Tissue Engineering Scaffolds, in *Green Polymer Composites Technology*, ed. S. Inamuddin, CRC Press, Boca Raton, 2016, pp. 343–354.

11 K. Huang, J. Wu and Z. Gu, *ACS Appl. Mater. Interfaces*, 2019, **11**, 2908–2916.

12 J. Huang, L. Chen, Q. Yuan, Z. Gu and J. Wu, *J. Biomed. Nanotechnol.*, 2019, **15**, 1371–1383.

13 J. Shi, A. R. Votruba, O. C. Farokhzad and R. Langer, *Nano Lett.*, 2010, **10**, 3223–3230.

14 Y. L. Colson and M. W. Grinstaff, *Adv. Mater.*, 2012, **24**, 3878–3886.

15 H. Liu, E. B. Slamovich and T. J. Webster, *Nanotechnology*, 2005, **16**, S601.

16 K. Goto, J. Tamura, S. Shinzato, S. Fujibayashi, M. Hashimoto, M. Kawashita, T. Kokubo and T. Nakamura, *Biomaterials*, 2005, **26**, 6496–6505.

17 H. Tiainen, D. Wiedmer and H. J. Haugen, *J. Eur. Ceram. Soc.*, 2013, **33**, 15–24.

18 E. Fidancevska, G. Ruseska, J. Bossert, Y. M. Lin and A. R. Boccaccini, *Mater. Chem. Phys.*, 2007, **103**, 95–100.

19 S. S. Samandari, H. Yekta, S. Ahmadi and K. Alamara, *Int. J. Biol. Macromol.*, 2018, **106**, 481–488.

20 C. H. Tiainen, J. C. Wohlfahrt, A. Verket, S. P. Lyngstadaas and H. J. Haugen, *Acta Biomater.*, 2012, **8**, 2384–2391.

21 M. Kulkarni, A. Mazare, E. Gongadze, A. Perutkova, V. Kralj-Iglic, I. Milošev, P. Schmuki, A. Igli and M. Mozetič, *Nanotechnology*, 2015, **26**, 1–18.

22 L. Cano, E. Pollet, L. Avérous and A. Tercjak, *Appl. Sci. Manuf.*, 2017, **93**, 33–40.

23 A. R. Ikono, N. Li, N. H. Pratama, A. Vibriani, D. R. Yuniarni, M. Luthfansyah, B. M. Bachtiar, E. W. Bachtiar, K. Mulia, M. Nasikin, H. Kagami, X. Li, E. Mardliyati, N. T. Rochman, T. Nagamura-Inoue and A. Tojo, *Biotechnol. Rep.*, 2019, **24**, e00350.

24 A. R. Costa-Pinto, A. M. Martins, M. J. Castelhano-Carlos, V. M. Correlo, P. C. Sol, A. Longatto-Filho, M. Battacharya, R. L. Reis and N. M. Neves, *J. Bioact. Compat. Polym.*, 2014, **29**, 137–151.

25 Q. Hou, D. W. Grijpma and J. Feijen, *Biomaterials*, 2003, **24**, 1937–1947.

26 Y. S. Nam and T. G. Park, *J. Biomed. Mater. Res.*, 1999, **47**, 8–17.

27 A. S. K. Kiran, T. S. Sampath Kumar, R. Sanghavi, M. Doble and S. Ramakrishna, *Nanomaterials*, 2018, **8**, 860.

28 C. Tang, C. D. Saquing, J. R. Harding and S. A. Khan, *Macromolecules*, 2010, **43**, 630–637.

29 N. E. P. Ismaya, M. Diantoro, A. Kusumaatmaja and K. Triyana, *Mater. Sci. Eng.*, 2017, **202**, 012011.

30 K. O. Kim, Y. Akada, W. Kai, B. S. Kim and I. S. Kim, *J. Biomater. Nanobiotechnol.*, 2011, **2**, 353–360.

31 T. Jamnongkan, A. Wattanakornsiri, P. P. Pansila, C. Migliaresi and S. Kaewpirom, *Adv. Mater. Res.*, 2012, **463–464**, 734–738.

32 N. T. B. Linh and B. T. Lee, *J. Biomater. Appl.*, 2012, **27**(3), 255–266.

33 H. Adeli, M. T. Khorasani and M. Parvazinia, *Int. J. Biol. Macromol.*, 2019, **1**, 238–254.

34 S. Chahal, F. S. J. Hussain, A. Kumar, M. S. B. A. Rasad and M. M. Yusoff, *Chem. Eng. Sci.*, 2016, **22**, 17–29.